Performance of dispersed Rayleigh interferometer on the active cophasing and alignment testbed

Shanshan Wang (王姗姗)*, Qiudong Zhu (朱秋东), Weirui Zhao (赵伟瑞), Lin Li (李 林), and Genrui Cao (曹根瑞)

Department of Optoelectronic Engineering, Beijing Insititute of Technology, Beijing 100081, China

**E-mail: lilunwuli5@bit.edu.cn*

Received February 10, 2009

We report the laboratory experiment on a segmented mirror testbed that shows the use of a dispersed Rayleigh interferometer to phase segmented mirrors. Segment alignment of tip-tilt is fulfilled by overlapping diffraction pattern centroids of the three individual segments on the focal plane. A spherical interferometer is introduced to evaluate the performance of piston, tip-tilt sensing, and control closed-loop, and finally a total residual root-mean-square (RMS) surface error of about 45 nm is achieved, in which a typical error of about 20 nm is contributed by piston. These results demonstrate that the dispersed Rayleigh interferometer can successfully sense the piston of segmented mirrors and be used in phasing segmented telescopes under extensive studies.

OCIS codes: 120.3180, 120.1088, 120.2830, 120.6085.

doi: 10.3788/COL20090711.1007.

We report a laboratory experiment to demonstrate the use of a dispersed Rayleigh interferometer (DRI) to cophase a segmented mirror. DRI is explored to measure the optical path difference (OPD) between two parallel beams, and is shown to be able to detect phasing error generated by a pair of transmissive phase plates in the range of 200 μm with a repeatability of 2 nm and reach an accuracy of 6.56 nm in 1-μm range[1]. Because of its high resolution, large dynamic range, and compactness, it was proposed as a cophasing sensor for segmented mirrors[2].

As the required sensing and real-time control accuracy of cophasing and alignment of segmented mirrors is typically a small fraction of a wavelength[3], which equals several tens of nanometers in optical spectrum range, it is one of the most difficult and also key technologies in the new generation telescopes[4]. Therefore, segmented-mirror testbeds are established to validate wavefront sensing (including piston, tip-tilt, and high order abberations) and control algorithms, for example, the famous wavefront sensing and control testbed (WCT)[5] and active phasing experiment (APE)[6]. There are also some segmented mirror testbeds in China, such as the "experiment system of the segmented-mirror active optics" in Nanjing Astronomical Instruments Research Center[7] which is used to validate real-time control algorithms, the "segmented mirror system with three sub-mirrors primary" in Harbin Institute of Technology[8,9] which helps the study of synthetic aperture optics theory and image quality evaluation, and the "active cophasing and alignment testbed (ACAT)" in Beijing Institute of Technology established in 2008 aiming to validate piston, tip-tilt sensing, and real-time control algorithms.

The phasing experiments reported here were carried out on ACAT in closed-loop mode. The optical configuration of ACAT is shown in Fig. 1. It consists of the source module, the beam splitting module, the segmented mirror module, the piston detection module (i.e., DRI), the tip-tilt detection module, a FOTO plane interferometer, and a FISBA spherical interferometer.

A 10-μm pinhole was illuminated by a fiber bundle connected to a continuous spectrum tungsten filament light source. Then the wave from the pinhole was collimated to provide a point source at infinity. After the beam splitting module, the plane wave was converged and reflected to the segmented mirror. A spherical mirror with a spherical radius of 1500 mm and a caliber of about 330 mm was divided into 3 segments. The first segment

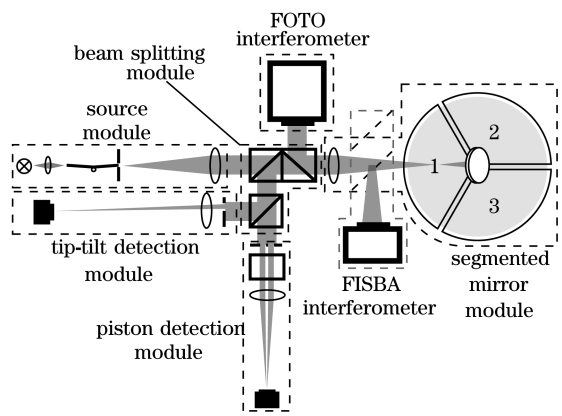

Fig. 1. Optical configuration of ACAT.

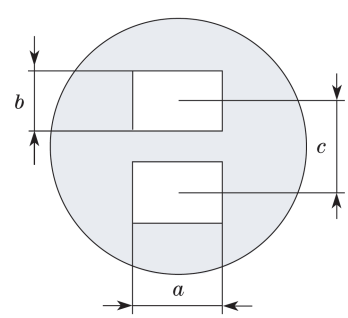

Fig. 2. Parameters of DRI aperture stop in ACAT, a=6 mm, b=4 mm, and c=6 mm.

(Seg. 1) was fixed and the other two were adjustable respectively in 3 degrees of freedom (piston, tip, and tilt) using piezoelectric transducer (PZT) actuators with a stoke of 25 μm. Waves reflected from the segmented mirror were re-collimated and then incident to the piston detection module and tip-tilt detection module. Seg. 1 was taken as reference, errors of Seg. 2 and Seg. 3 were detected respectively by rotating the aperture stop and then the control module gave orders to the actuators according to the error signal. After several iterations, the piston and tip-tilt error signals of both Seg. 2 and Seg. 3 went steadily to zero. Then the FISBA interferometer was introduced by inserting a flat mirror to evaluate the performance of the piston and tip-tilt detection-correction closed-loop.

DRI consists of aperture stop, Amici prism, imaging lens, and complementary metal oxide semiconductor (CMOS). In ACAT, the aperture stop of DRI, as shown in Fig. 2, is placed on the exit-pupil plane on which the image size of segmented mirror is about 25 mm in diameter.

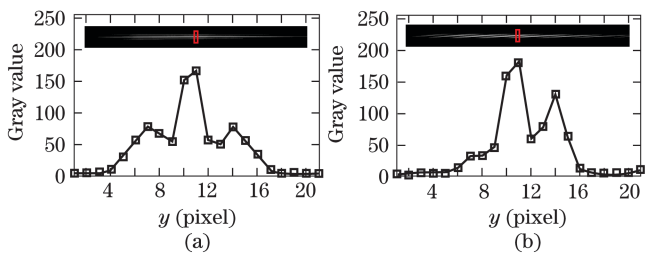

Fig. 3. Intensity distributions along y axis and 2D DRIPs insets. (a) OPD=0, (b) OPD=–16803 nm.

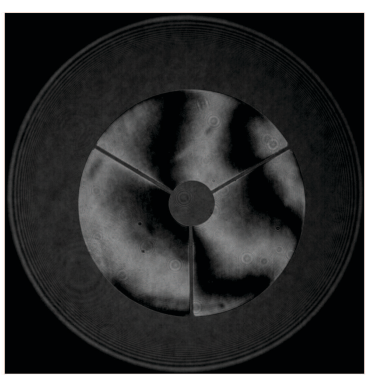

Fig. 4. Original interferogram of FISBA interferometer after closed-loop correction. PV=0.50λ, RMS=0.07λ, global tip-tilt and defocus are removed, λ=632.8 nm. Relative residual local tip-tilt errors between the three segments are typically PV=0.06λ, and the individual segments figure error is about PV=0.24λ, RMS=0.03λ.

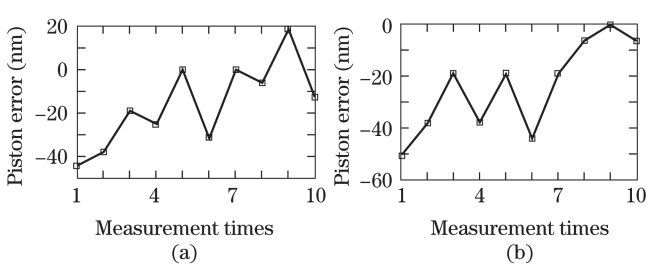

Fig. 5. Accuracy of piston measurement-correction. (a) Seg. 2, (b) Seg. 3.

The focal length of the imaging lens is 180 mm, and the pixel size of detector is 5.2 μm, that means the main lobe of dispersed Rayleigh interference pattern (DRIP) takes up only about 3.5 pixels when λ=590 nm. The Amici prism disperses the monochromatic Rayleigh interference patterns (MRIPs) along the x direction into 401 columns in the range of 516–668 nm determined by tungsten filament light source spectrum and CMOS quantum efficiency (QE) range. The intensity distribution of DRIPs acquired on ACAT is shown in Fig. 3.

As detailed in Ref. [1], the intensity distribution of DRIP along the y axis is

$$I(y) = 2S(\lambda)B^2\left(\frac{y}{\lambda f}\right)\left\{1+\gamma\cos\left[2\pi\left(\frac{\delta}{\lambda}+cy\right)\right]\right\}, \quad (1)$$

where $S(\lambda)$ is the spectral intensity, $B^2\left(\frac{y}{\lambda f}\right)$ is the intensity distribution along the y axis corresponding to a single hole of the DRI aperture stop, $x(\lambda)$ describes the dispersive character of the Amici prism, and $\gamma \in [0,1]$ is the visibility, which is related to the dispersive power and OPD. We have proposed a data processing method – two-dimensional fringe analyzing (2D-FA)[2], which contains three steps to analyze DRIPs. The first step is calculating the decimal fraction OPD $\delta_d(\lambda)$ of each wavelength, the second one is eliminating 2π ambiguity, and the third step is averaging the OPD detected by each wavelength $\delta(\lambda)$ to improve accuracy. Different from Ref. [2], in ACAT, we use the ratio of main lobe energy to total energy in a column to determine the decimal fraction OPD $\delta_d(\lambda)$ instead of using the main lobe centroid offset, mainly because three positions to be detected share one set of DRI by rotating. Moreover, the width of main lobe of 3.5 pixels is not enough for using frequency domain filtering to calibrate the absolute zero position with an acceptable accuracy.

We started our correction loop after placing the mirror in a perturbed position. Typical figures for the piston, tip, and tilt wavefront perturbations are several microns (peak to valley, PV). Then we run correction iterations to drive the mirror to minimize piston, tip, and tilt signals until the root-mean-square (RMS) signal of the wave front sensor was converged. After the closed-loop control of Seg. 2 and Seg. 3, the FISBA spherical interferometer was introduced. The obtained interferogram is shown in Fig. 4.

We repeated the process for 10 times, and achieved typical values of PV= 0.50λ and RMS=0.07λ. From the interferogram, we can intuitively see that the segmented-mirror figure error and the optical system error contribute more to the whole aperture PV and RMS values, instead of alignment and cophasing error. Consequently, the piston error is discussed independently. Piston errors of Seg. 2 and Seg. 3 are shown in Fig. 5.

The residual piston RMS typically achieved is 18.6 nm, less than 20 nm. These results give the first laboratory demonstration, to our knowledge, that the DRI can measure and correct segment misalignments of piston to an accuracy of 20 nm working in broadband light. Moreover, we notice that most of the detected piston errors are negative, especially for Seg. 3. We believe that this is caused by the segmented-mirror figure error and the sampling area difference between DRI and FISBA.

The authors thank Dr. X. Hu for providing tip-tilt control program and the support during the experiment.

References

1. S. Wang, Q. Zhu, and G. Cao, Proc. SPIE **7283,** 72833G (2009).
2. S. Wang, Q. Zhu, and G. Cao, Acta Opt. Sin. (in Chinese) **29,** 2435 (2009).
3. A. Schumacher, N. Devaney, and L. Montoya, Appl. Opt. **41,** 1297 (2002).
4. D. Su and X. Cui, Progress in Astronomy (in Chinese) **17,** 1 (1999).
5. C. Bowers, P. Davila, B. Dean, B. Perkins, M. Wilson, D. Redding, S. Basinger, D. Cohen, A. Lowman, F. Shi, L. Burns, M. Fitzmaurice, T. Norton, P. Petrone, and L. Wheeler, Proc. SPIE **4013,** 763 (2000).
6. F. Gonte, N. Yaitskova, F. Derie, A. Constanza, R. Brast, B. Buzzoni, B. Delabre, P. Dierickx, C. Dupuy, R. Esteves, C. Frank, S. Guisard, R. Karban, E. Koenig, J. Kolb, M. Nylund, L. Noethe, I. Surdej, A. Courteville, R. Wilhelm, L. Montoya, M. Reyes, S. Esposito, E. Pinna, K. Dohlen, M. Ferrari, and M. Langlois, Proc. SPIE **5894,** 58940Z (2005).
7. D. Su, W. Zou, Z. Zhang, Y. Qu, and S. Yang, Proc. SPIE **4003,** 417 (2000).
8. W. Zhang, J. Deng, F. Long, M. Zhao, and B. Zuo, Acta Opt. Sin. (in Chinese) **28,** 687 (2008).
9. W. Long, Z. Wang, and Y. Zhou, Acta Opt. Sin. (in Chinese) **24,** 1009 (2004).